

Closed-loop tracking control of a pendulum-driven cart-pole underactuated system

H Yu^{1*}, Y Liu¹, and T Yang²

¹Faculty of Computing, Engineering, and Technology, Staffordshire University, Stafford, UK

²School of Engineering and Information Technology, Sussex University, Brighton, UK

The manuscript was received on 4 July 2007 and was accepted after revision for publication on 15 November 2007.

DOI: 10.1243/09596518JSCE460

Abstract: This paper investigates a new modelling and control issue: the tracking control problem of underactuated dynamic systems by using a special example – a pendulum-driven cart-pole system. A dynamic model of a pendulum-driven cart-pole system is firstly presented. Then, a six-step motion strategy of the pendulum-driven cart-pole system is proposed. After that, a desired profile of the pendulum joint velocity is developed based on the proposed six-step motion strategy. The desired joint position and acceleration can be computed using the desired joint velocity profile. A closed-loop control approach is proposed using the partial feedback linearization technique. Finally, extensive simulation studies are conducted to demonstrate the proposed approaches.

Keywords: underactuated dynamic systems, tracking control, stabilization, inverted pendulum

1 INTRODUCTION

In the past two decades, the analysis and control of fully actuated robot manipulators has been extensively studied. Many control strategies based on passivity, Lyapunov theory, feedback linearization, adaptability, robustness, learning, etc. [1], have been developed for the fully actuated case, i.e. systems with the same number of actuators as degrees of freedom. The techniques developed for fully actuated robot manipulators do not apply directly to the case of underactuated non-linear mechanical systems. Underactuated mechanical systems [2, 3] or underactuated vehicles are systems with fewer independent control actuators than degrees of freedom to be controlled. In recent years there has been a major interest in developing stabilizing algorithms for underactuated mechanical systems [4, 5]. The need for analysis and control of underactuated mechanical systems arises in many practical applications. The interest comes from the need to stabilize systems like ships, underwater vehicles,

helicopters, aircraft, satellites, mobile robots, space platforms, flexible joint robots, hyper-redundant and snake-like manipulators, walking robots, capsule robots, and hybrid machines, which may be underactuated by design or become underactuated due to actuator failure.

The classical inverted pendulum mounted on a cart is a benchmark underactuated system that has been widely used in many control laboratories to demonstrate the effectiveness of different control approaches in a manner analogous to the control of many real systems. The control issue requires not only stabilization of the pendulum in the upward equilibrium position but also has to consider the displacement of the cart, and this will certainly increase the design complexity. There are many similar extended systems, such as Acrobot [6], Pendubot [7], double inverted pendulum [8], three-link gymnast robot [9], Furuta pendulum [10, 11], and reaction wheel pendulum [12], which belong to the class of underactuated mechanical systems. For controlling nonlinear underactuated mechanical systems, many control strategies such as the Lyapunov method [13], sliding mode control [14], and adaptive robust control [15] have been extensively

*Corresponding author: Faculty of Computing, Engineering, and Technology, Staffordshire University, Stafford ST16 9DG, UK. email: h.yu@staffs.ac.uk

studied. However, control of underactuated systems has been mainly along the line of stabilization of special examples of cascade non-linear systems using linearization-based methods or energy-based methods [3, 11].

This paper describes an experiment contrary to the classical inverted pendulum cart (cart-pole) system [16]. Here the pendulum-driven cart using torque on the pivot is considered, instead of the force on the cart. The difference between the classical cart-driven system and the pendulum-driven system is that the former addresses a stabilization problem and the latter addresses a tracking problem. The aim of the cart-driven inverted pendulum is to rotate the pendulum to the upward position and stabilize it there by applying a control input force to the cart [16], while the aim of the pendulum-driven inverted pendulum is to make the cart trajectory track a desired (designed) trajectory by applying a control input torque to the pendulum.

This paper investigates the tracking control problem [17, 18] of underactuated dynamic systems by using an example – the pendulum-driven cart-pole system [19]. A four-step motion, dynamic modelling, and optimal open-loop control of the pendulum-driven cart-pole system is investigated in reference [19]. Optimization and control of a pendulum-driven cart-pole system are investigated in reference [20]. An initial experimental study using the open-loop control strategy is conducted in reference [21]. In this paper, a six-step motion strategy of the pendulum-driven cart-pole system is proposed. A desired profile of the pendulum joint velocity is proposed based on the proposed six-step motion strategy. The desired joint position and acceleration can be computed by using the desired joint velocity profile. A closed-loop control approach is proposed by using the partial feedback linearization technique [3, 4] and its robust performance has been discussed. The desired joint trajectory will be used in the proposed control approach. An optimal parameter selection is also investigated. Extensive simulation studies are conducted to demonstrate the proposed approaches and its robustness.

2 DYNAMIC MODELLING OF A PENDULUM-DRIVEN CART

2.1 Generic models of underactuated systems

A generic model of the dynamics of an n -DOF (degrees of freedom) system [1, 3–5] can be written

as

$$\mathbf{D}(\mathbf{q})\ddot{\mathbf{q}} + \mathbf{C}(\mathbf{q}, \dot{\mathbf{q}})\dot{\mathbf{q}} + \mathbf{G}(\mathbf{q}) + \mathbf{u}_d = \mathbf{B}\mathbf{u} \quad (1)$$

where $\mathbf{q} \in \mathcal{R}^n$ is a vector of the generalized coordinates, $\mathbf{D}(\mathbf{q}) \in \mathcal{R}^{n \times n}$ is the inertia matrix, $\mathbf{C}(\mathbf{q}, \dot{\mathbf{q}})\dot{\mathbf{q}} \in \mathcal{R}^n$ represents the centripetal and Coriolis forces, $\mathbf{G}(\mathbf{q})$ represents the gravitational forces, $\mathbf{u}_d \in \mathcal{R}^n$ is the external disturbances, $\mathbf{u} \in \mathcal{R}^r$ is the vector of control input, and $\mathbf{B} \in \mathcal{R}^{n \times r}$. If $r = \text{rank}(\mathbf{B}) = n$, the system represented by equation (1) is called a full-actuated system, which has been investigated intensively during the past two decades. If $r = \text{rank}(\mathbf{B}) < n$, the system represented by equation (1) is called an underactuated system. Without losing the generality, let $\mathbf{B} = [0 \ \mathbf{I}_m]^T$ and $\mathbf{q} = [\mathbf{q}_1^T \ \mathbf{q}_2^T]^T$, where $\mathbf{q}_1 \in \mathcal{R}^{n-r}$ and $\mathbf{q}_2 \in \mathcal{R}^r$. Equation (1) can be written as

$$\begin{aligned} \mathbf{D}_{11}\ddot{\mathbf{q}}_1 + \mathbf{D}_{12}\ddot{\mathbf{q}}_2 + \mathbf{h}_1(\mathbf{q}_1, \dot{\mathbf{q}}_1, \mathbf{q}_2, \dot{\mathbf{q}}_2) &= 0 \\ \mathbf{D}_{21}\ddot{\mathbf{q}}_1 + \mathbf{D}_{22}\ddot{\mathbf{q}}_2 + \mathbf{h}_2(\mathbf{q}_1, \dot{\mathbf{q}}_1, \mathbf{q}_2, \dot{\mathbf{q}}_2) &= \mathbf{u} \end{aligned} \quad (2)$$

where \mathbf{h}_i includes terms of the centripetal, Coriolis forces, the gravitational forces, and the external disturbances.

2.2 Modelling of a pendulum-driven cart-pole system

The pendulum-driven cart-pole system is shown in Fig. 1. The inverted pendulum is mounted on the top of the cart. The cart has four passive wheels, which make it move horizontally on the ground. A torque motor is directly attached to the pivot on the cart to swing the pendulum. M is the mass of the cart, m is the mass of the ball, l is the distance between the pivot and the ball centre, μ is the friction coefficient between the cart and the ground, θ is the pendulum angle from vertical, x is the cart position coordinate, and τ is the torque applied to the pivot by the motor.

Let the centre of the cart be the origin of the coordinate. Thus the coordinate of the ball is

$$[x_b \ y_b]^T = [x - l \sin\theta \ \ l \cos\theta]^T$$

Let $F = [F_x \ F_y]^T$ be the internal force applied to the pendulum by the torque. From Newton's law, summing the forces applied on the ball in the horizontal direction gives $F_x = -m\ddot{x}_b$ and summing the forces applied on the ball in the vertical direction gives

$$F_y - mg = m\ddot{y}_b$$

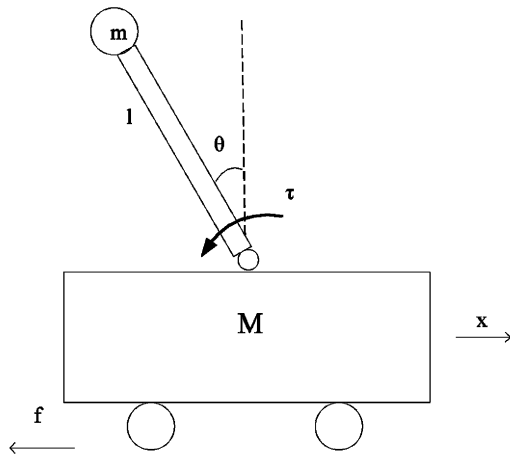


Fig. 1 Pendulum-driven cart-pole system

Combining the two equations gives

$$F = \begin{bmatrix} F_x \\ F_y \end{bmatrix} = \begin{bmatrix} -m\ddot{x} + ml\ddot{\theta} \cos\theta - ml\dot{\theta}^2 \sin\theta \\ mg - ml\ddot{\theta} \sin\theta - ml\dot{\theta}^2 \cos\theta \end{bmatrix}$$

Thus the torque can be calculated as

$$\tau = [l \cos\theta \quad -l \sin\theta] \cdot F = -ml\ddot{x} \cos\theta + ml^2\ddot{\theta} - mgl \sin\theta$$

Then summing the forces applied on the cart in the horizontal direction gives

$$F_x - f = M\ddot{x}$$

where $f = \mu N \operatorname{sgn}(\dot{x})$ is the friction force of the cart on the ground. Summing the forces applied on the cart in the vertical direction gives the normal force

$$N = Mg + F_y = (M + m)g - ml\ddot{\theta} \sin\theta - ml\dot{\theta}^2 \cos\theta$$

Summarizing the above, the dynamical model is given as

$$\begin{aligned} (M + m)\ddot{x} - ml\ddot{\theta}(\mu \sin\theta \operatorname{sgn} \dot{x} + \cos\theta) \\ + ml\dot{\theta}^2(\sin\theta - \mu \cos\theta \operatorname{sgn} \dot{x}) \\ + \mu(M + m)g \operatorname{sgn} \dot{x} = 0 \end{aligned} \quad (3)$$

$$(-ml \cos\theta)\ddot{x} + (ml^2)\ddot{\theta} - mgl \sin\theta = \tau \quad (4)$$

Let $q_1 = x$, $q_2 = \theta$, and $u = \tau$. Equations (3) and (4) can be written in a general compact form

$$D_{11}\ddot{q}_1 + D_{12}\ddot{q}_2 + h_1(q_1, \dot{q}_1, q_2, \dot{q}_2) = 0$$

$$D_{21}\ddot{q}_1 + D_{22}\ddot{q}_2 + h_2(q_1, \dot{q}_1, q_2, \dot{q}_2) = u$$

where $D_{11} = M + m$, $D_{12} = -ml(\cos q_2 + \mu \sin q_2 \operatorname{sgn} \dot{q}_1)$, $D_{21} = -ml \cos q_2$, $D_{22} = ml^2$, $h_1 = ml(\sin q_2 - \mu \cos q_2 \operatorname{sgn} \dot{q}_1)\dot{q}_2^2 + \mu(M + m)g \operatorname{sgn} \dot{q}_1$, and $h_2 = -mgl \sin q_2$.

The control goal is to drive the cart to move in one direction only by adjusting the control input τ . It is noted that the control goal of the classical cart-pendulum system is to make the origin globally asymptotically stable [16].

3 MOTION GENERATION ANALYSIS

To drive the cart to move in one direction by using the joint torque only, two stages can be defined: (1) fast motion stage: moving the pendulum in one direction fast leads to $F_x \gg f_{\max}$, where f_{\max} is the maximal dry friction of the cart along the x axis, therefore making the cart move, and (2) slow motion stage: returning the pendulum to its starting position slowly which makes $|F_x| < |f_{\max}|$, which will keep the cart still. By using this philosophy, the desired joint velocity profile shown in Fig. 2 can be generated, where θ_d is the desired joint velocity that the system needs to track.

The details of the motion profile are given below.

1. $t \in [0, t_1]$. The motion with a high angular acceleration of the pendulum ($\ddot{\theta} \gg 0$, $\dot{\theta} > 0$) leads to the forward accelerated motion of the cart ($\ddot{x} > 0$, $\dot{x} > 0$).
2. $t \in [t_1, t_2]$. The motion with an angular deceleration of the pendulum ($\ddot{\theta} < 0$, $\dot{\theta} > 0$) leads to the forward decelerated motion of the cart ($\ddot{x} < 0$, $\dot{x} > 0$).
3. $t \in [t_2, t_3]$. The motion with a low angular deceleration of the pendulum ($-\varepsilon < \ddot{\theta} < 0$, $\dot{\theta} > 0$) leads to the cart remaining stationary ($\ddot{x} = 0$, $\dot{x} = 0$), where ε is the critical value of angular acceleration to keep the cart stationary.
4. $t \in [t_3, t_4]$. The motion with a low angular acceleration of the pendulum ($-\varepsilon < \ddot{\theta} < 0$, $-\omega_2 < \dot{\theta} < 0$) in a very short duration leads to the cart remaining stationary ($\ddot{x} = 0$, $\dot{x} = 0$).
5. $t \in [t_4, t_5]$. The motion with a zero acceleration and a low constant angular velocity of the pendulum ($\ddot{\theta} = 0$, $\dot{\theta} = -\omega_2$) leads to the cart remaining stationary ($\ddot{x} = 0$, $\dot{x} = 0$).
6. $t \in [t_5, t_6]$. The motion with a low angular deceleration of the pendulum ($0 < \ddot{\theta} < \varepsilon$, $-\omega_2 < \dot{\theta} < 0$) in a very short duration leads to the cart remaining stationary ($\ddot{x} = 0$, $\dot{x} = 0$).

The cycle time $T = t_6$. For one full cycle, the motion strategy includes two types: fast motion

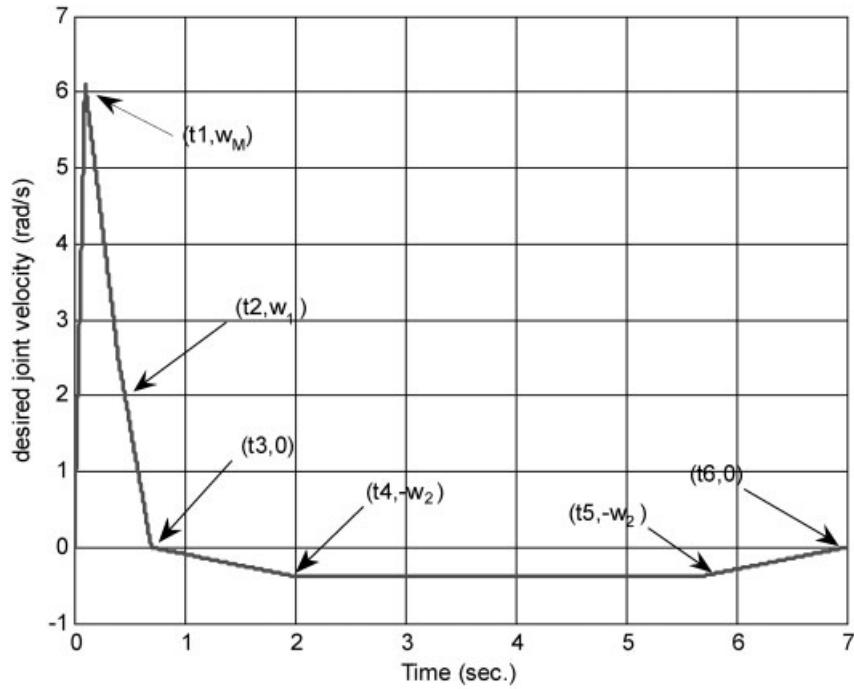


Fig. 2 Desired joint velocity profile for one cycle

(steps 1 and 2) and slow motion (steps 3 to 6). Following the above, the formula for the desired joint velocity is given by

$$\dot{\theta}_d(t) = \begin{cases} \frac{t}{t_1} w_M, & t \in [0, t_1) \\ w_M - \frac{t-t_1}{t_2-t_1} (w_M - w_1), & t \in [t_1, t_2) \\ \frac{t_3-t}{t_3-t_2} w_1, & t \in [t_2, t_3) \\ \frac{t_3-t}{t_4-t_3} w_2, & t \in [t_3, t_4) \\ -w_2, & t \in [t_4, t_5) \\ \frac{t_6-t}{t_5-t_6} w_2, & t \in [t_5, t_6) \end{cases} \quad (5)$$

Remark 1

From Fig. 2, for $0 < t < t_3$, the joint has moved in a positive direction. Therefore, the initial position of the joint ($-\theta_0$) must be negative. Also, the positive area of the desired joint velocity ($0 < t < t_3$) must be less than $(\pi/2 + \theta_0)$.

Using the desired joint velocity from system (5), the trajectories of the desired joint position and the acceleration can be computed. Figure 3 shows the desired joint position (θ_d) profile obtained from system (5). To make the cart move forward every cycle, several constraints should be considered. The pendulum-driven cart-pole system must satisfy those constraints, which will be discussed in the next section.

4 SYSTEM CONSTRAINTS AND OPEN-LOOP OPTIMAL CONTROL STRATEGY

4.1 System constraints

4.1.1 Constraint for the whole motion

In order to keep the cart on the ground, the normal force of the cart on the ground has to be greater than zero, i.e.

$$Mg + F_y = (M + m)g - ml\ddot{\theta} \sin\theta - ml\dot{\theta}^2 \cos\theta > 0$$

Lemma 1

If the following inequality is satisfied

$$\ddot{\theta}^2 + \dot{\theta}^4 < \sigma^2 \quad (6)$$

where $\sigma = (M + m)g/ml$, the constraint $Mg + F_y > 0$ will be satisfied, i.e. the cart will be on the ground.

Proof

Using the constraint of the normal force of the cart on the ground

$$\ddot{\theta} \sin\theta + \dot{\theta}^2 \cos\theta < (M + m)g/(ml)$$

Then, let $\alpha = \arccos\ddot{\theta} / \sqrt{\ddot{\theta}^2 + \dot{\theta}^4}$ that satisfies

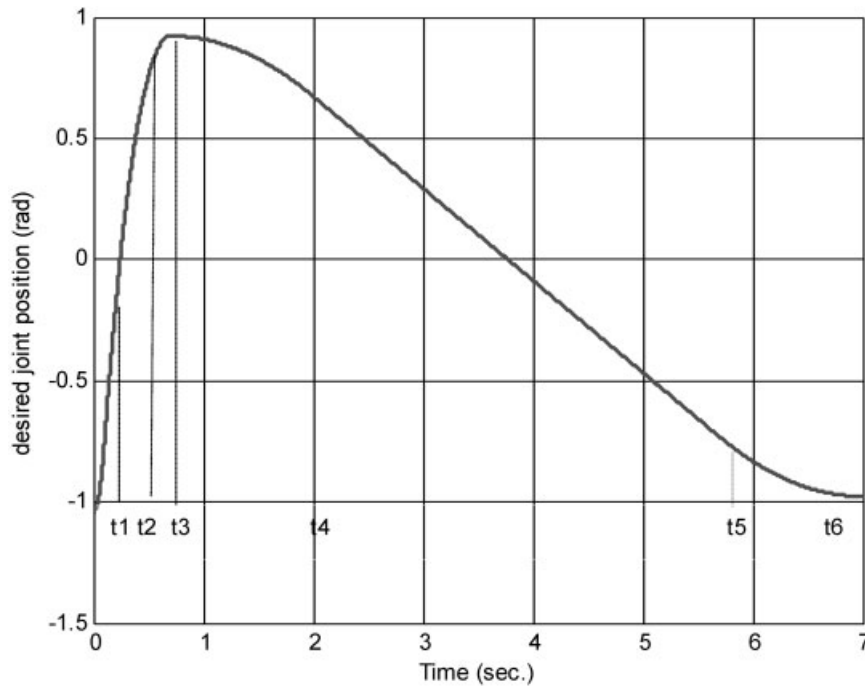


Fig. 3 Desired joint position profile for one cycle

$$\sqrt{\ddot{\theta}^2 + \dot{\theta}^4} \sin(\theta + \alpha) < (M + m)g / (ml)$$

Enlarging the inequality leads to the sufficient condition. It should be considered that $\sqrt{\ddot{\theta}^2 + \dot{\theta}^4} \leq \sqrt{\ddot{\theta}^2 + \dot{\theta}^4} \sin(\theta + \alpha) < \sigma$, i.e. $\ddot{\theta}^2 + \dot{\theta}^4 < \sigma^2$.

4.1.2 Constraint for the slow motion (steps 3 to 6)

During the slow motion, in order to keep the cart stationary, the internal force in the horizontal direction has to be lower than the maximal dry friction force, i.e. $|F_x| \leq \mu(Mg + F_y)$.

Lemma 2

If the following inequality is satisfied

$$\ddot{\theta}^2 + \dot{\theta}^4 < \left(\frac{\mu\sigma}{1+\mu}\right)^2 \tag{7}$$

the constraint $|F_x| \leq \mu(Mg + F_y)$ will be satisfied, i.e. the cart will be stationary. Also, the constraint for the whole motion will be held.

Proof

Using the expression of the forces in horizontal and vertical directions and the fact that the cart is

stationary in slow motion

$$\begin{aligned} & |ml\ddot{\theta} \cos\theta - ml\dot{\theta}^2 \sin\theta| \\ & \leq \mu(Mg + mg - ml\ddot{\theta} \sin\theta - ml\dot{\theta}^2 \cos\theta) \end{aligned}$$

Taking out the absolute sign and considering one side of the inequality

$$\begin{aligned} & ml(\ddot{\theta} \cos\theta - \dot{\theta}^2 \sin\theta) \\ & \leq \mu(M + m)g - \mu ml(\ddot{\theta} \sin\theta + \dot{\theta}^2 \cos\theta) \end{aligned}$$

select a constant $\beta = \arccos(\ddot{\theta} / \sqrt{\ddot{\theta}^2 + \dot{\theta}^4})$ that satisfies

$$\sqrt{\ddot{\theta}^2 + \dot{\theta}^4} \cos(\theta + \beta) + \mu \sqrt{\ddot{\theta}^2 + \dot{\theta}^4} \sin(\theta + \beta) < \mu\sigma$$

Enlarging the inequality gives the sufficient condition

$$\begin{aligned} (1 + \mu) \sqrt{\ddot{\theta}^2 + \dot{\theta}^4} & < \sqrt{\ddot{\theta}^2 + \dot{\theta}^4} \cos(\theta + \beta) \\ + \mu \sqrt{\ddot{\theta}^2 + \dot{\theta}^4} \sin(\theta + \beta) & < \mu\sigma \end{aligned}$$

i.e. $\ddot{\theta}^2 + \dot{\theta}^4 < [\mu\sigma / (1 + \mu)]^2$. Using the same method on another side of the inequality can generate the same result.

An alternative expression of the constraint by using torque τ is

$$\begin{aligned} & \frac{-\mu(M+m)gl + ml^2\dot{\theta}^2(\sin\theta + \mu\cos\theta)}{\cos\theta - \mu\sin\theta} \\ & \leq \tau + mgl\sin\theta \\ & \leq \frac{\mu(M+m)gl + ml^2\dot{\theta}^2(\sin\theta - \mu\cos\theta)}{\cos\theta + \mu\sin\theta} \end{aligned}$$

For a given friction coefficient μ , $\theta_0 \in (-\phi, \phi)$ should be chosen that make both $\cos\theta - \mu\sin\theta$ and $\cos\theta + \mu\sin\theta$ greater than zero, and satisfies $-\tan^{-1}(1/\mu) < \phi < \tan^{-1}(1/\mu)$.

4.2 Open-loop control strategy

From the discussion in section 3, it is known that the motion in one full cycle can be classified as fast motion (steps 1 and 2) and slow motion (the rest of the steps). During the fast motion, the cart moves forward ($\dot{x} > 0$) all the time. Because the duration of each step is fixed, using equations (3) and (4) the desired acceleration of the cart for steps 1 and 2 for each sampling time can be computed as

$$\ddot{x}_d = \frac{ml\ddot{\theta}_d(\cos\theta_d + \mu\sin\theta_d) - ml\dot{\theta}_d^2(\sin\theta_d - \mu\cos\theta_d)}{M+m} - \mu g$$

and the desired torque as

$$\tau = -ml\ddot{x}_d \cos\theta_d + ml^2\ddot{\theta}_d - mgl\sin\theta_d \text{ for } t \in [0, t_2] \quad (8)$$

where θ_d is the desired joint position, $\ddot{\theta}_d$ is the desired joint acceleration, and both of them are computed from the desired joint velocity $\dot{\theta}_d$.

Using system (5) and considering that $\ddot{x} = 0$ in equation (4), the desired torque for steps 3 and 4 can be computed as

$$\tau = \begin{cases} -\frac{w_1 ml^2}{t_3 - t_2} - mgl\sin\theta_d, & t \in [t_2, t_3) \\ -\frac{w_2 ml^2}{t_4 - t_3} - mgl\sin\theta_d, & t \in [t_3, t_4) \end{cases} \quad (9)$$

During step 5, $\dot{x} = 0$, $\ddot{x} = 0$, $\ddot{\theta} = 0$, then

$$\tau = -mgl\sin\theta_d, \quad t \in [t_4, t_5) \quad (10)$$

During step 6, the desired torque is

$$\tau = \frac{w_2 ml^2}{t_6 - t_5} - mgl\sin\theta_d, \quad t \in [t_5, t_6] \quad (11)$$

The open-loop control law is given by equations (8) to (11). This has been adopted in references [19] and [20].

4.3 Optimal open-loop control strategy

The aim of the optimization is to maximize the average speed of the cart by choosing the desired joint velocity profile. Here there are several parameters that should be designed, such as $t_1 \sim t_6$, w_M , w_1 , and w_2 in the motion profile shown in Fig. 2. The following boundary conditions can be followed

$$\theta_0 > 0, \theta(0) = -\theta(t_2) = -\theta_0, \dot{\theta}(0) = 0, \dot{x}(0) = \dot{x}(t_2) = 0$$

Integrating equation (3) in $[0, t_2]$ and using the above boundary conditions lead to the following two equations

$$\begin{aligned} (M+m)\dot{x} - ml\dot{\theta}\cos\theta - \mu ml\dot{\theta}\sin\theta &= -\mu(M+m)gt \\ &= ml(\sin\theta_0 + \mu\cos\theta_0) - 1/2\mu(M+m)gt^2 \end{aligned} \quad (12)$$

$$\begin{aligned} (M+m)x - ml\sin\theta + \mu ml\cos\theta \\ &= ml(\sin\theta_0 + \mu\cos\theta_0) - 1/2\mu(M+m)gt^2 \end{aligned} \quad (13)$$

Using equation (12) and considering that $ml(\cos\theta_0 + \mu\sin\theta_0) \neq 0$ (θ_0 can be chosen to avoid this), at time t_2 , w_1 is

$$w_1 = \dot{\theta}(t_2) = \frac{\mu(M+m)gt_2}{ml(\cos\theta_0 + \mu\sin\theta_0)} \quad (14)$$

From Fig. 2, there are the following relations

$$1/2 w_M t_1 + 1/2 (w_M + w_1)(t_2 - t_1) = 2\theta_0$$

$$1/2 [(t_6 - t_3) + (t_5 - t_4)] w_2 = 2\theta_0 + 1/2 w_1 (t_3 - t_2)$$

Thus, this leads to

$$w_M = \frac{4\theta_0 + w_1(t_1 - t_2)}{t_2} \quad (15)$$

$$w_2 = \frac{4\theta_0 + w_1(t_3 - t_2)}{t_6 + t_5 - t_4 - t_3} \quad (16)$$

Using system (5) the desired joint position and acceleration can be computed. It is noted that

$$w_M t_2 + w_1(t_3 - t_1) = w_2(t_5 + t_6 - t_3 - t_4)$$

The above equation can be used to select the difference between t_4 and t_5 as

$$t_5 - t_4 = \frac{1}{w_2} [w_M t_2 + w_2(t_3 - t_6) + w_1(t_3 - t_1)] \quad (17)$$

Using equation (13) and considering the boundary conditions, at time t_2 , gives

$$x(t_2) = \frac{2m}{M+m} l \sin \theta_0 - \frac{1}{2} \mu g t_2^2 \quad (18)$$

It can be found that if the duration of the fast motion is shorter (i.e. t_2 is smaller), the cart will move further (i.e. $x(t_2)$ is larger). The desired torque for such a velocity profile can be computed using equations (8) to (11). The average velocity of the cart is

$$\dot{x} = \frac{x(t_2)}{T} = \left[2ml \sin \theta_0 / (M+m) - \mu g t_2^2 / 2 \right] t_6$$

Thus if $t_1 = 0.1$ s, $t_2 = 0.4$ s, $t_3 = 0.6$ s, $t_4 = 1.4$ s, $t_6 - t_5 = 0.8$ s are given, w_1 , w_2 , w_M , and $t_5 - t_4$ can be computed using equations (14) to (17). This will generate a significant difference in terms of the distance that the cart can travel in the same length of time. This has been demonstrated by the simulation study.

5 CLOSED-LOOP CONTROL USING PARTIAL FEEDBACK LINEARIZATION

From equation (3)

$$\begin{aligned} \ddot{x} = \frac{1}{M+m} \{ & ml[\cos \theta + \mu \sin \theta \operatorname{sgn}(\dot{x})] \ddot{\theta} \\ & - ml[\sin \theta - \mu \cos \theta \operatorname{sgn}(\dot{x})] \dot{\theta}^2 \\ & - \mu(M+m)g \operatorname{sgn}(\dot{x}) \} \end{aligned}$$

The control law is proposed using the partial feedback linearization as

$$\tau = \alpha u + \beta \quad (19)$$

where

$$\alpha = ml^2 - \frac{m^2 l^2}{M+m} \cos \theta (\cos \theta + \mu \sin \theta \operatorname{sgn} \dot{x})$$

$$\begin{aligned} \beta = \frac{ml}{M+m} \cos \theta \left[ml(\sin \theta - \mu \cos \theta \operatorname{sgn} \dot{x}) \dot{\theta}^2 \right. \\ \left. + \mu(M+m)g \operatorname{sgn} \dot{x} \right] - mgl \sin \theta \end{aligned}$$

Letting $\tilde{\theta} = \theta - \theta_d$, choosing

$$u = \ddot{\theta}_d - K_v \dot{\tilde{\theta}} - K_p \tilde{\theta}$$

and applying control law (19) to equation (4) give the error equation as

$$\ddot{\tilde{\theta}} + K_v \dot{\tilde{\theta}} + K_p \tilde{\theta} = 0 \quad (20)$$

The suitable values of K_v and K_p can be designed using the standard linear control theory to make the joint follow the desired profile.

6 SIMULATION STUDY

6.1 Simulation results

The simulation was carried out by using MATLAB/Simulink. All of the relative parameters are given as $M = 0.5$ kg, $m = 0.05$ kg, $L = 0.3$ m, $\mu = 0.01$ N/m s, and $g = 9.81$ m/s². To avoid the condition when $\dot{x} = 0$ in the simulation study, the following friction model is used

$$f = \begin{cases} \mu N \operatorname{sgn}(\dot{x}), & \dot{x} \neq 0 \\ \mu N \operatorname{sgn}(F_x), & \dot{x} = 0 \end{cases}$$

Because of the accuracy requirement, the open-loop control sampling interval is selected at 1 ms, and a desired torque plus the corrective torque is applied on the joint, i.e.

$$\tau = \tau_d + \tau_e$$

where τ_d is the desired torque given by equations (8) to (11), and τ_e is the corrective torque. Because of the nature of open-loop control, the system will fail when using τ_d only. Therefore, here an additional torque is used to compensate for the inaccuracy caused by computation errors. In other words, the open-loop control should be adjusted before the successful application. The selection procedures for the additional torque are described below.

First simulate the system using the desired torque τ_d . At each failed point, the desired torque is slightly adjusted based on the failed simulation results to maintain the joint velocity tracking around the

desired joint velocity profile. After several trials, the corrective torque can be found.

Figure 4 shows the results of the open-loop control strategy presented in section 4.2 in a full cycle. From Fig. 4(c), it can be seen that the joint velocity of the pendulum has small tracking errors with the desired joint velocity because of the

corrective torque (τ_e). Figure 5 shows the cart movement in five cycles.

Figures 6 and 7 show the simulation results when the optimal parameters are adopted. Comparing Fig. 5 and Fig. 7 reveals that the cart travels about 17 cm in less than 13 s under the optimal control, while it takes about 35 s to travel less than 13 cm

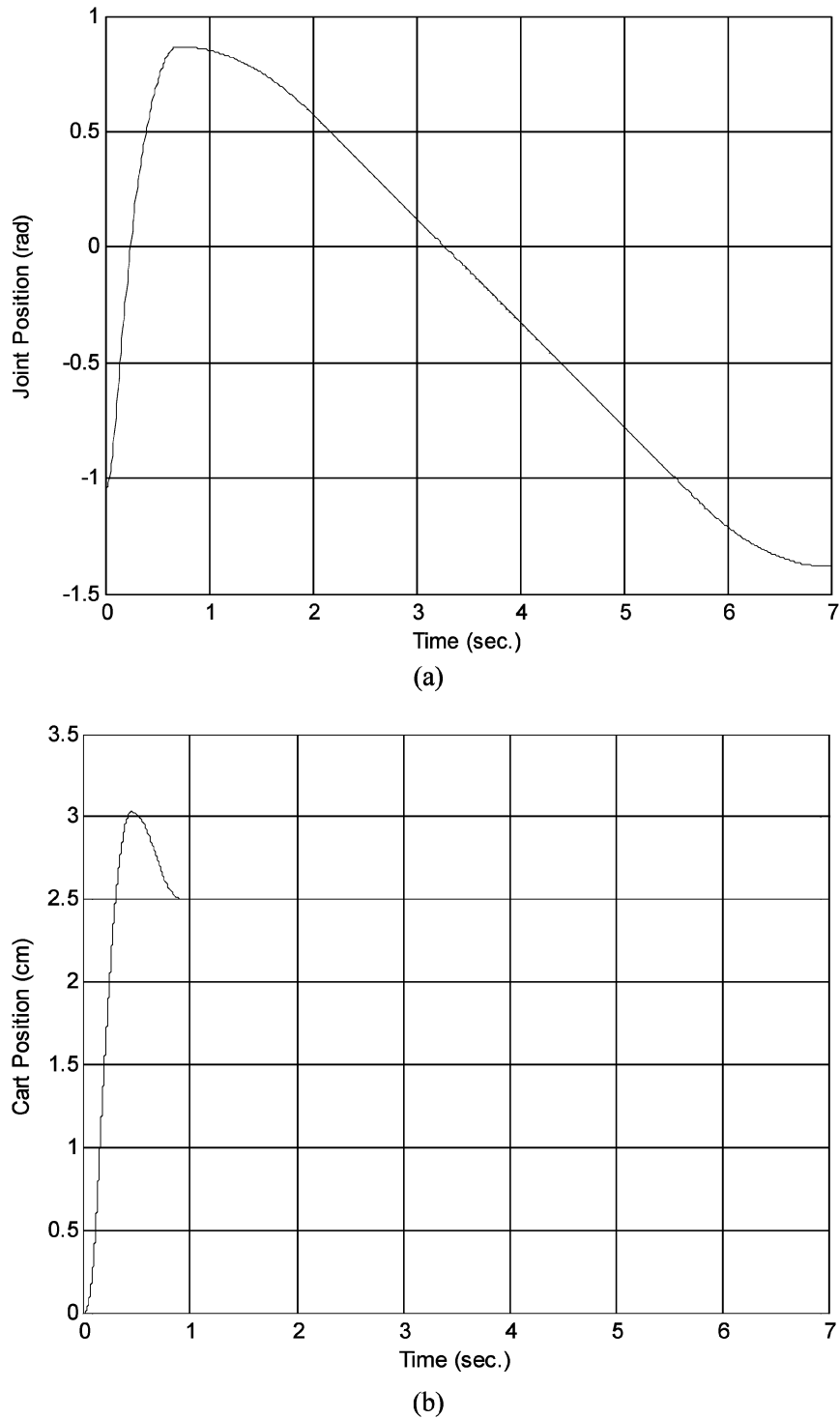
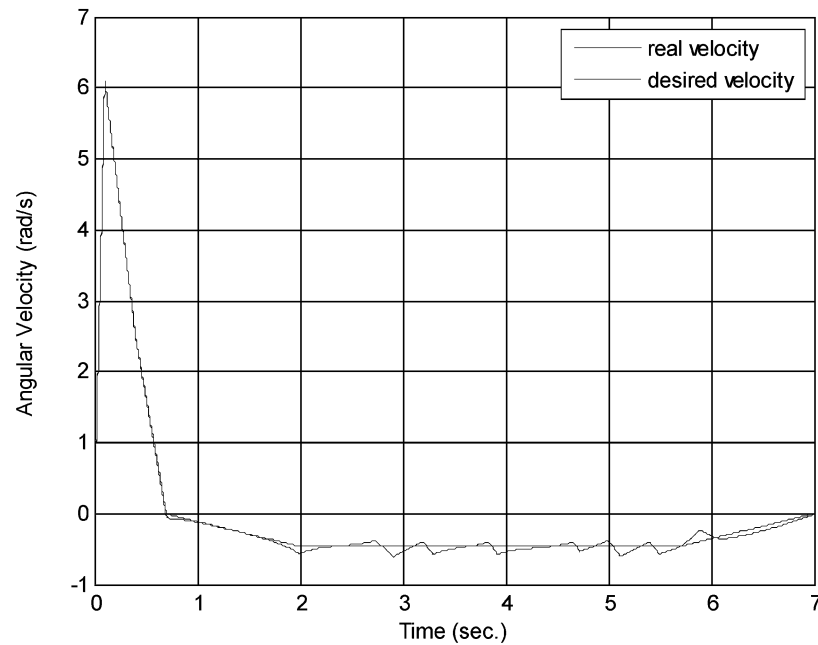
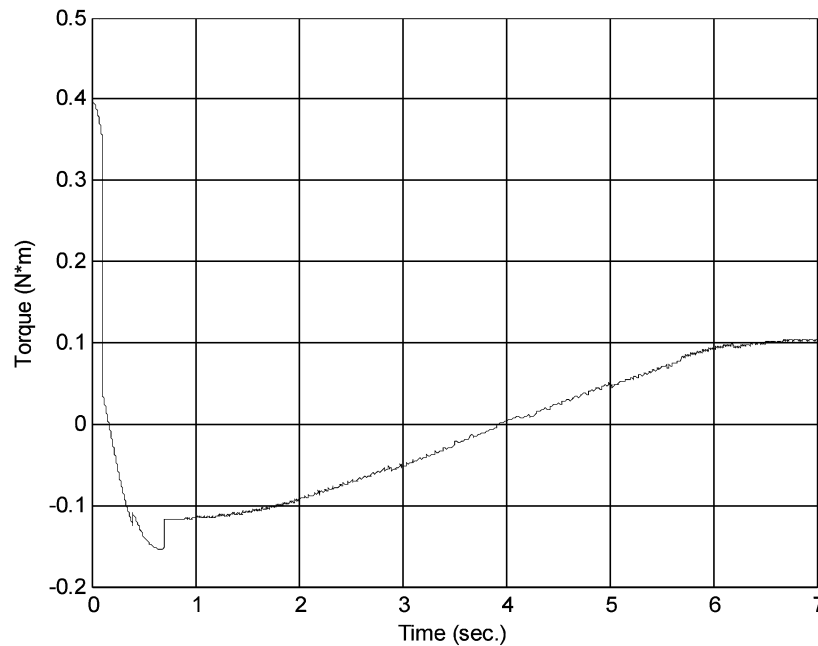


Fig. 4 One full cycle of the pendulum-driven cart-pole system



(c)



(d)

Fig. 4 (Continued)

under the non-optimal control. To make a fair comparison, the control inputs for both cases are shown in Fig. 4(d) and Fig. 6(b). The optimal control does require slightly more energy.

Figure 8 shows the cart position and control input for one full stroke (one cycle) within a 10 ms sampling interval. The cart moves about 3.5 cm in one cycle. Figure 9 shows the cart position and control input for five full strokes. The cart moves about 17 cm in five cycles using less than 13 s. The

pendulum joint tracking performance in Fig. 10 shows that the joint position and velocity are almost the same as the designed profile.

6.2 Robust test

Due to the existing modelling error, the open-loop control strategy will fail to control the system, since it is sensitive to error. The simulation results

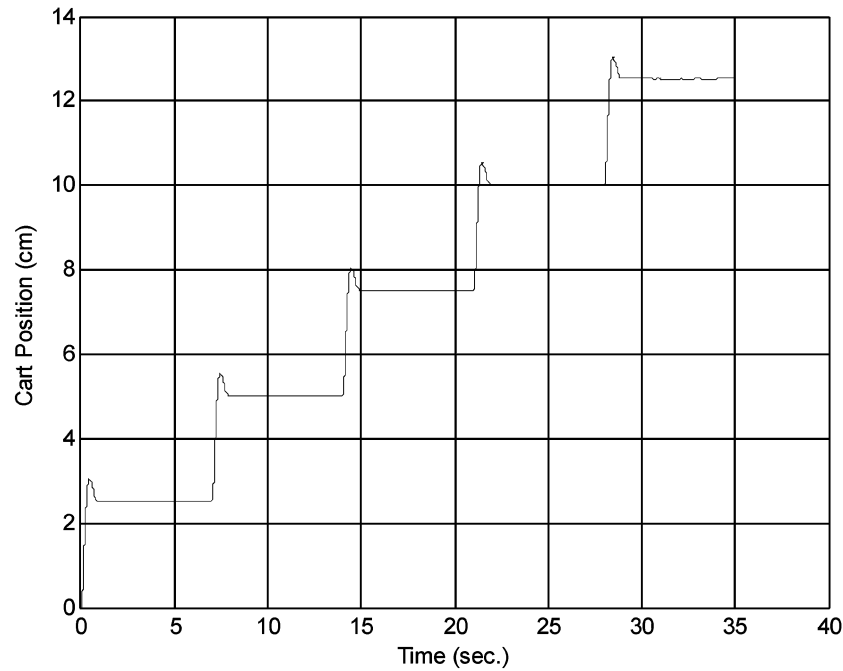


Fig. 5 Cart trajectory in five cycles

demonstrate that the open-loop control strategy only works in an ideal case.

To test the performance of the proposed closed-loop strategy, a variable disturbance is added on the system parameters as

$$\rho' = \rho[1 + \lambda \sin(\omega t)]$$

where ρ represents the parameters M , m , L , and μ ; λ is the variable rate; and ω is the variable frequency.

Figure 11 shows the results of the parameter uncertainties using the closed-loop control law. Figure 11(a) shows the variable disturbance on the cart mass which is carried out at 0~30, 0~50, and 0~80 per cent respectively. In this case, the cart may move forward since the constraint (7) for the slow motion is not satisfied. Variable disturbance on the pendulum mass is carried out at 0~10, 0~30, and 0~50 per cent respectively in Fig. 11(b). The results show that the ball mass is too sensitive to be controlled. Because of the term $\sigma = (M+m)g/(ml)$ in constraint (7), small changes on the ball mass or the pendulum length will cause the change of boundary in constraint (7). The variable disturbance on the pendulum length causes the cart to move backwards at 0~50 per cent disturbance in Fig. 11(c). Figure 11(d) shows that the proposed closed-loop control strategy has a better performance against the disturbance of μ . However, the Coulomb friction model is used in this paper. In real experiments, the static friction is always twice the

kinetic friction. Due to the modelling error on the friction, the tracking performance of the pendulum will not be disturbed. The cart will not move at the beginning of step 1; with the change of internal forces, the cart will be driven when the constraint $|F_x| \leq \mu(Mg + F_y)$ is not satisfied. Therefore the trajectory of the cart will be affected, which can make the average speed of the cart lower.

7 CONCLUSIONS

The paper has investigated the tracking issue of underactuated dynamic systems. A special example, a pendulum-driven cart-pole system, has been considered to demonstrate the proposed concepts. The paper has three contributions: (1) a six-step motion profile; (2) an optimal parameter selection procedure; (3) a closed-loop control law and its robust analysis. The extensive simulations conducted have demonstrated the proposed approaches.

Comparing the results with reference [19], it is shown that the input profile used in reference [19] is in linear form, while the input profile used in this paper is non-linear. The linear input profile [19] shows that the pendulum is stable anywhere without any control input, which makes the experiment easier but not in a general way. The linear input is easier to implement in experimental work, but it is hard to decide on the input rate and the results are

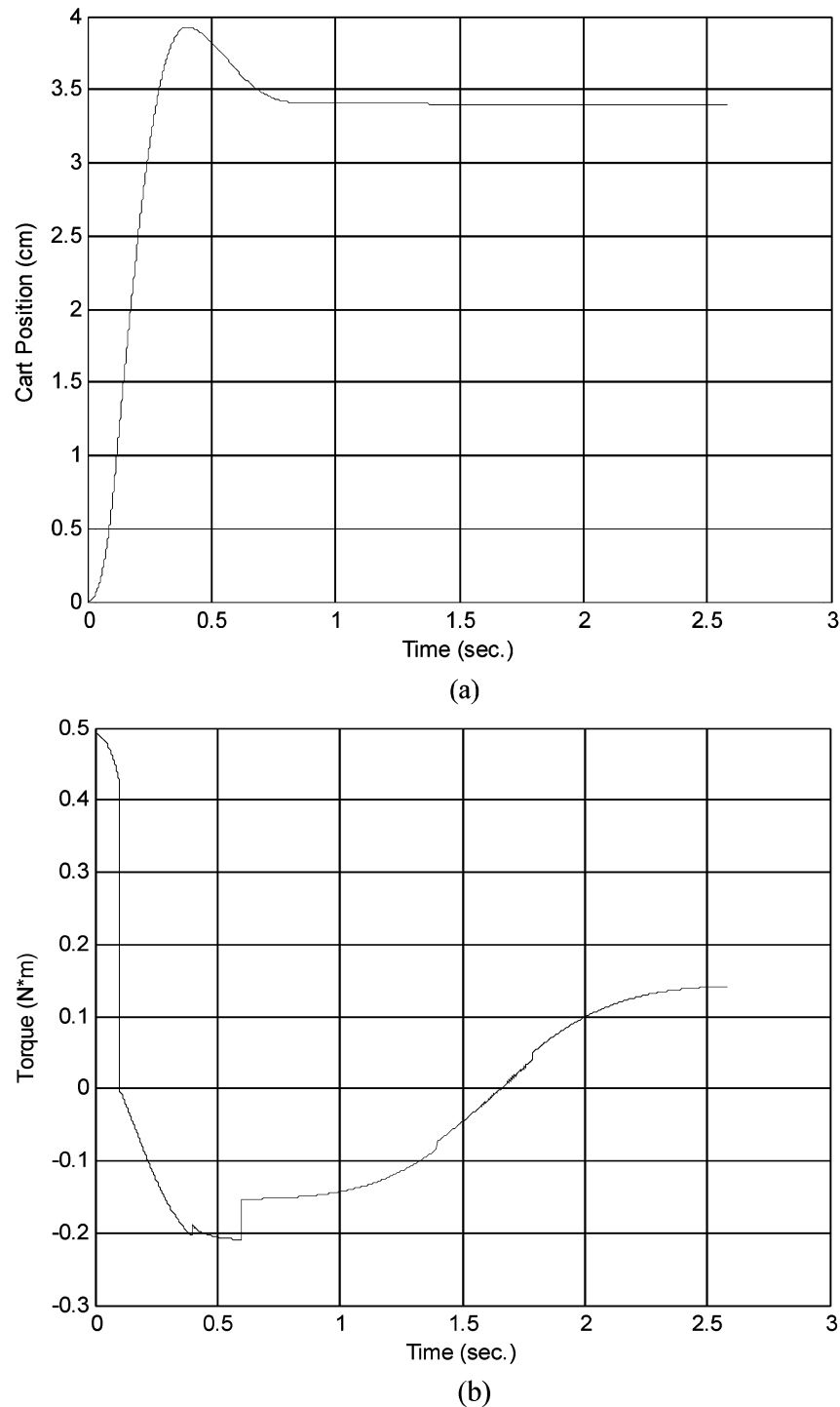


Fig. 6 Results of the pendulum-driven cart system with the optimal configuration in a full cycle

unpredictable. The simulation results in this paper demonstrate that the open-loop control cannot be used directly on the experimental rig, since it is sensitive to disturbance. Based on this conclusion, this paper dispatches the idea of controlling the system using the closed-loop technique. On the other hand, the simulation results in this paper

cannot be compared with reference [19] because the experiment description in reference [19] is oversimple without any introduction of the experimental setup. However, the system parameters have a significant effect on the movement of the cart.

The lab-based device [21] consists of four passive wheels, which are tracked by using optical encoders

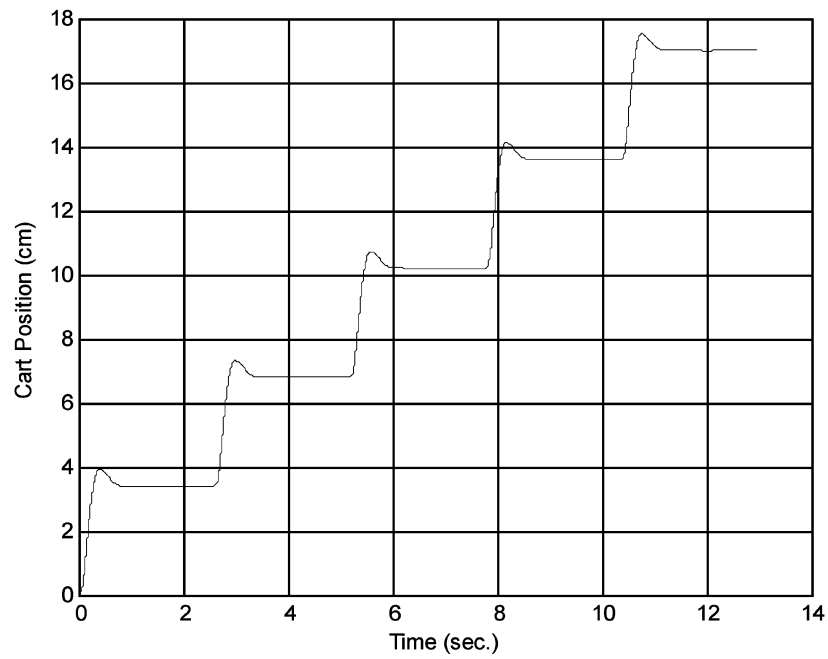


Fig. 7 Cart trajectory with the optimal configuration in five cycles

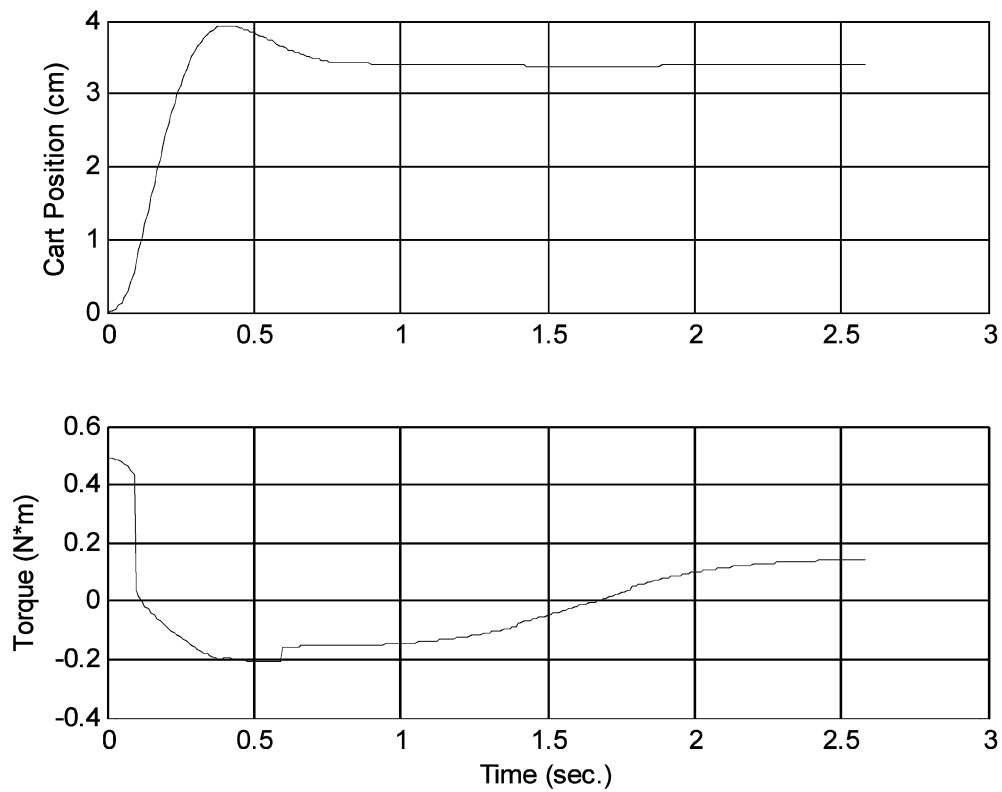


Fig. 8 Trajectories of the cart position and control input for one cycle of the closed-loop control

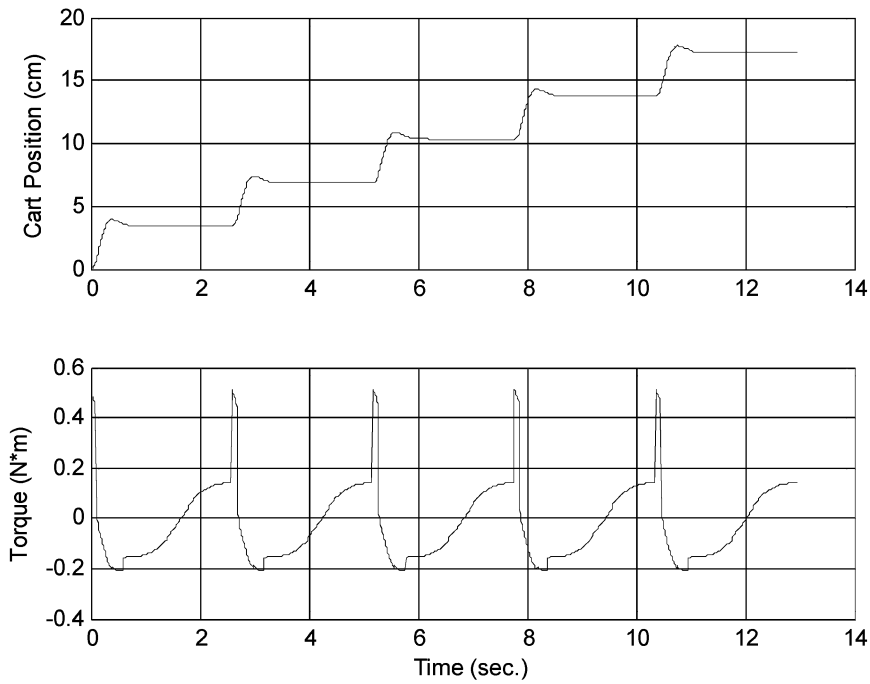


Fig. 9 Trajectories of the cart position and control input for five cycles of the closed-loop control

and a motor-driven inverted pendulum with a mass. The system is used as a test bed to demonstrate the reaction theory, allowing researchers to try out different control algorithms and view the movement of the pendulum and the cart over time. The

further improvement of the lab system is under development. The results will be published in due course.

The research aim is to develop an active-driven capsule robot which is small enough for people to

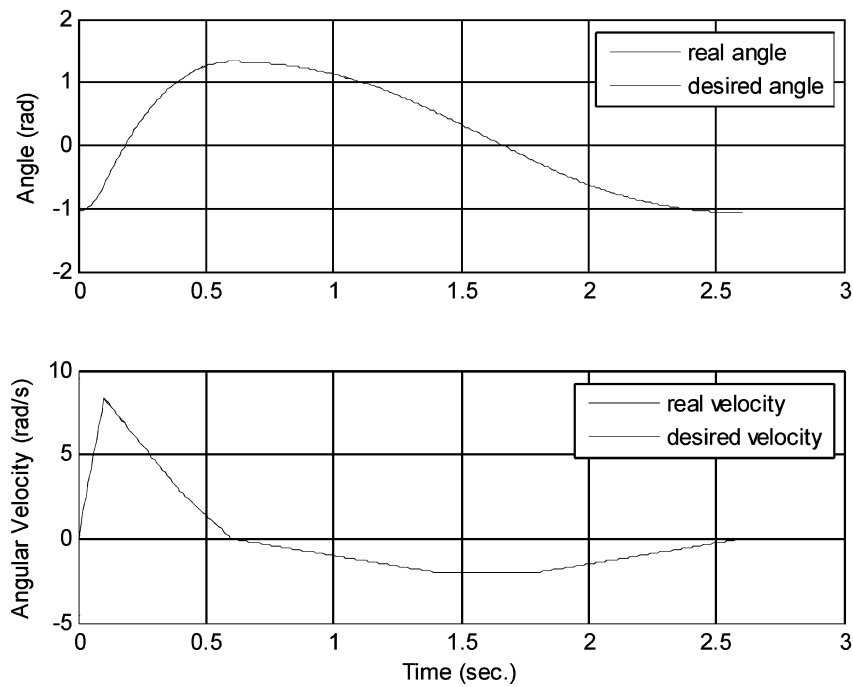
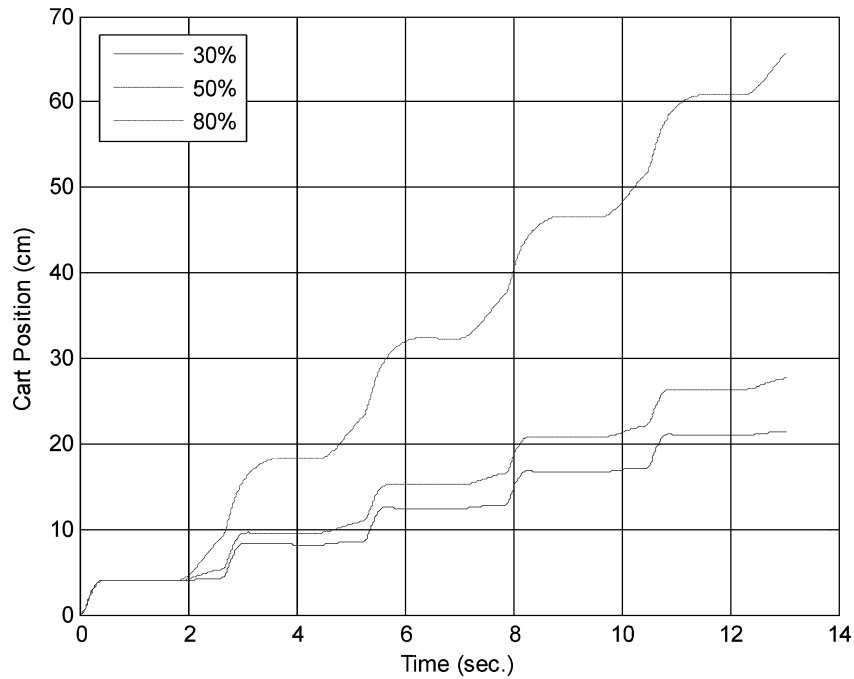
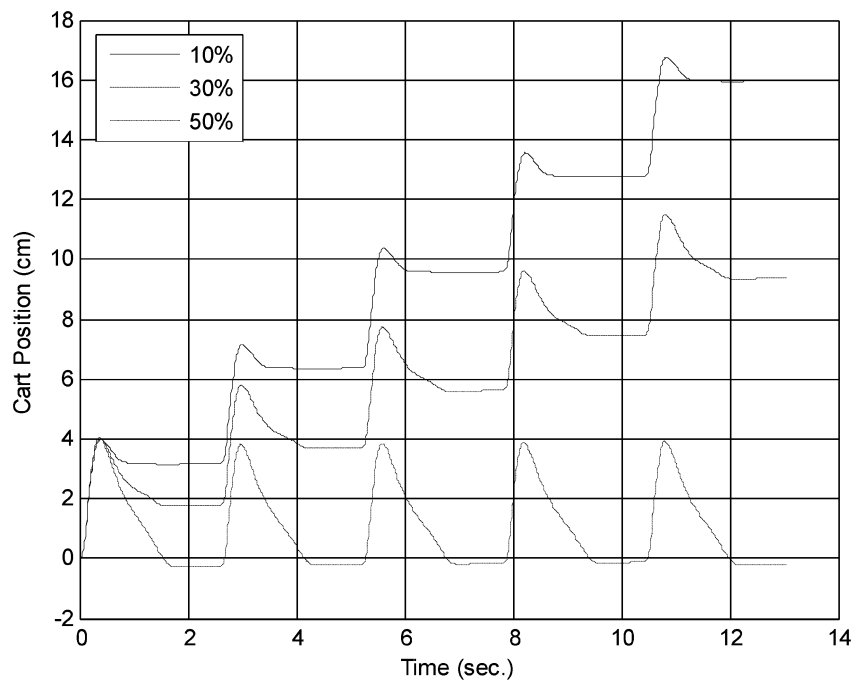
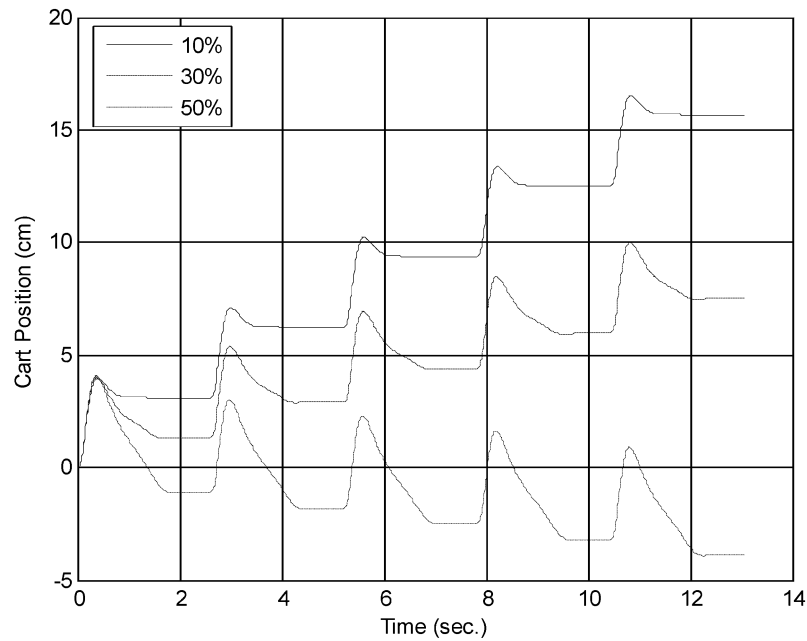
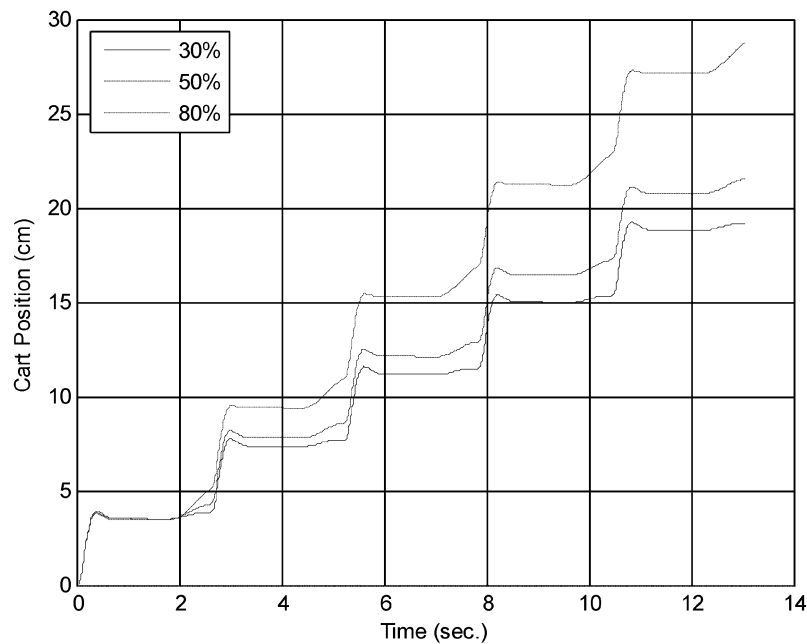


Fig. 10 Tracking performance of the joint velocity of the closed-loop control

(a) Variable disturbance on M (b) Variable disturbance on m **Fig. 11** Results of variable disturbance on system parameters using the closed-loop control

swallow, and use the idea developed here on the capsule robot to control its locomotion. The novel propulsion mechanism would have extensive applications for micro-robots in the

fields of medical inspection [22], engineering diagnosis, collapse rescue [23], etc. Briefly, the mechanism can be used as an autonomous mobile robot to inspect areas inaccessible to humans.

(c) Variable disturbance on L (d) Variable disturbance on μ **Fig. 11** (Continued)

Further work in this direction is under way and the research findings will be reported in due course.

(Research Grant EP/E025250/1) for the support of this research.

ACKNOWLEDGEMENTS

The authors would like to thank the Engineering and Physical Sciences Research Council (EPSRC)

REFERENCES

- 1 Spong, M. W., Lewis, F. L., and Abdallah, C. T. *Robot control – dynamics, motion planning and analysis*, 1993 (IEEE, Inc., New York).

- 2 **Spong, M. W.** Underactuated mechanical systems in control problems in robotics and automation. In *LNCIS* (Eds B. Siciliano and K. P. Valavanis), vol. 230, 1998, pp. 135–150 (Springer-Verlag, London).
- 3 **Aneke, N. P. I.** *Control of underactuated mechanical systems*. PhD Thesis, Mechanical Engineering Department, TU Eindhoven, 2003.
- 4 **Lozano, R.** and **Fantoni, I.** *Non-linear control for underactuated mechanical systems*, 2001 (Springer-Verlag, Berlin).
- 5 **Ortega, R., Spong, M. W., Gomez-Estern, F., and Blankenstein, G.** Stabilization of a class of underactuated mechanical systems via interconnection and damping assignment. *IEEE Trans. Autom. Control*, 2002, **47**(8), 1218–1233.
- 6 **Inoue, A., Deng, M., Hara, S., and Henmi, T.** Swing-up and stabilizing control system design for an Acrobot. In Proceedings of the IEEE International Conference on *Networking, sensing and control*, London, April 2007, pp. 559–561.
- 7 **Zhang, M.** and **Tarn, T.** Hybrid control of the Pendubot. *IEEE/ASME Trans. Mechatronics*, 2002, **7**(1), 79–86.
- 8 **Zhong, W.** and **Rock, H.** Energy and passivity based control of the double inverted pendulum on a cart. In Proceedings of the IEEE International Conference on *Control applications*, Mexico City, Mexico, September 2001, pp. 896–901.
- 9 **Takashima, S.** Control of gymnast on a high bar. In Proceedings of IROS'91 IEEE/RSJ International Workshop on *Intelligent robots and systems*, vol. 3, 1991, pp. 1424–1429.
- 10 **Aguilar-Ibanez, C., Gutierrez, O. F., and Sossa-Azuela, H.** Control of the Furuta pendulum by using a Lyapunov function. In Proceedings of the 45th IEEE Conference on *Decision and control*, 2006, pp. 6128–6132.
- 11 **Astrom, K. J.** and **Furuta, K.** Swinging up a pendulum by energy control. *Automatica*, February 2000, **36**(2), 287–295.
- 12 **Pathak, K., Franch, J., and Agrawal, S. K.** Velocity and position control of a wheeled inverted pendulum by partial feedback linearization. *IEEE Trans. Robotics*, June 2005, **21**(3), 505–513.
- 13 **White, W. N., Foss, M., and Guo, X.** A direct Lyapunov approach for a class of underactuated mechanical systems. In Proceedings of the 2006 American Control Conference, Minneapolis, Minnesota, June 2006, pp. 103–110.
- 14 **Nikkhah, M., Ashrafiuon, H., and Muske, K. R.** Optimal sliding mode control for underactuated systems. In Proceedings of the 2006 American Control Conference, Minneapolis, Minnesota, June 2006, pp. 4688–4693.
- 15 **Han, H.** A robust algorithm for model-following control of underactuated systems, and its application to a non-holonomic robot and an aircraft. *Int. J. Systems Sci.*, 2005, **36**(6), 341–356.
- 16 **Muskinja, N.** and **Tovornik, B.** Swinging up and stabilization of a real inverted pendulum. *IEEE Trans. Ind. Electronics*, April 2006, **53**(2), 631–639.
- 17 **Choudhury, P., Stephens, B., and Lynch, K. M.** Inverse kinematics-based motion planning for underactuated systems. In Proceedings of the IEEE International Conference on *Robotics and automation*, New Orleans, Louisiana, 2004, pp. 2242–2248.
- 18 **Jarzebowska, E.** Tracking control design for underactuated constrained systems. *Robotica*, 2006, **24**(5), 591–593.
- 19 **Li, H., Furuta, K., and Chernousko, F. L.** A pendulum-driven cart via internal force and static friction. In Proceedings of the Conference on *Physics and control*, St Petersburg, Russia, 2005, pp. 15–17.
- 20 **Liu, Y., Yu, H., and Burrows, B.** Optimization and control of a pendulum-driven cart-pole system. In Proceedings of the IEEE International Conference on *Networking, sensing and control*, London, April 2007, pp. 151–156.
- 21 **Wane, S. O., Yu, H., and Yang, T. C.** Development of a reaction drive for a propulsion mechanism. In Proceedings of the IEEE International Conference on *Networking, sensing and control*, London, April 2007, pp. 746–750.
- 22 **Karagozler, M. E., Cheung, E., Jiwoon, K., and Sitti, M.** Miniature endoscopic capsule robot using biomimetic micro-patterned adhesives. In Proceedings of the IEEE/RAS-EMBS International Conference on *Biomedical robotics and biomechanics*, 2006, pp. 105–111.
- 23 **Wilton, P.** Search and rescue. *Newsline EPRC Magazine*, Spring 2006, **36**, 05–32.

APPENDIX

Notation

B	matrix of external forces
C	matrix of centripetal and Coriolis forces
D	matrix of inertia
f_{\max}	the maximal dry friction of the cart along the x axis
F_x	internal force on the pendulum along the x axis
F_y	internal force on the pendulum along the y axis
G	gravitational forces
g	acceleration due to gravity
\mathbf{h}_i	terms of the centripetal, Coriolis forces, the gravitational forces, and the external disturbances
K_v	linear feedback gain of the joint velocity term
K_p	linear feedback gain of the joint position term

l	distance between the pivot and the ball centre	w_2	desired angular velocity of the pendulum during step 5
m	mass of the ball	x	coordinate of the cart in the x axis
M	mass of the cart	x_b	coordinate of the ball in the x axis
n	number of degree of freedoms	x_d	desired cart position
N	normal force on the ground	y_b	coordinate of the ball in the y axis
\mathbf{q}	vector of the generalized coordinates		
\mathbf{q}_1	unactuated configuration vectors	θ	pendulum angle
\mathbf{q}_2	actuated configuration vectors	$\tilde{\theta}$	error between the pendulum angle and the reference angle
r	number of actuators		
t_i	duration time of step i	θ_d	desired angle of the pendulum
T	cycle time	θ_0	initial pendulum angle
\mathbf{u}	vector of the control input	μ	friction coefficient between the cart and the ground
\mathbf{u}_d	vector of external disturbances		
w_M	desired angular velocity of the pendulum at t_1	τ	input torque
		τ_d	desired torque
w_1	desired angular velocity of the pendulum at t_2	τ_e	corrective torque
		ϕ	boundary of the pendulum position